Supplementary Material:

Stromal HIF2 Regulates Immune Suppression in the Pancreatic Cancer Microenvironment

Supplementary Methods:

Ex Vivo Analysis of Fibroblasts

Hif2α$^{fl/fl}$; *αSMA*$^{CreERT2/+}$; *tdTomato*$^{LSL/LSL}$ fibroblasts were treated with DMSO, 4-hydroxytamoxifen (4-OHT), or Adeno-Cre as a positive control. Fibroblasts were then genotyped as described previously[1] and imaged with an Olympus FV500 laser scanning confocal microscope (Olympus USA).

Histopathology, Immunohistochemistry, and Immunofluorescence

Spontaneous PDAC tumors were harvested from KPF CAF-HIF2 wild-type (WT) and knockout (KO) mice and fixed with 10% neutral buffered formalin, subjected to ethanol dehydration, washed in Histoclear (National Diagnostics, HS2001GLL), and embedded in paraffin. Then 5-μm-thick tissue slices were cut, mounted onto slides, and stained with H&E. Masson's trichrome staining was performed in the Research Histology Core Lab at MD Anderson. Histopathologic assessment of H&E staining and fibrosis scoring of trichrome-stained tumor slides were performed by a pathologist (J. Zhao) who was blinded to genotype.

Immunohistochemistry (IHC) was performed as previously described[2] using anti-HIF2α (1:200, Abcam ab199, RRID:AB_302739), anti-F4/80 (1:200, Abcam ab6640, RRID:AB_1140040), anti-Meca32 (1:200, Novus Biologicals NB100-77668, RRID:AB_1084448), and anti-FoxP3 (1:200, Abcam ab20034, RRID:AB_445284) antibodies. Slides were counterstained with Hematoxylin QS (Vector Laboratories, H3404-100, RRID:AB_2336843) and imaged with a BioTek Cytation 5 Cell Imaging Multi-Mode Reader (RRID:SCR_019732) or Leica Aperio CS2 digital pathology slide scanner. F4/80 and FoxP3 images were analyzed by quantifying the number of positively stained cells per field (20x). For vessel density analysis, the National Institutes of Health (NIH)'s ImageJ software (ImageJ, RRID:SCR_003070; Fiji, RRID:SCR_002285) was used with a custom macro to identify, mask, and determine %vessel coverage.

Immunofluorescence (IF) was performed using anti-HIF2α (1:200, Abcam ab199) and anti-αSMA (1:200, Abcam ab7817, RRID:AB_2223021) and secondary antibodies

goat anti-Rabbit Alexa Fluor 555 (1:200, ThermoFisher A-21429, RRID:AB_2535850) and goat anti-Mouse Alexa Fluor 488 (1:200, ThermoFisher A-11029, RRID:AB_2534088). Analysis was performed using National Institutes of Health ImageJ software with a custom macro to quantify relative fluorescent intensity of HIF2α in αSMA+ cells. Briefly, αSMA was used to define a binary cell mask that was applied to HIF2α images. Average fluorescent intensity of the mask images was subsequently recorded.

Generation of HIF2 KO CAF Cell Line

Please see "Isolation of Fibroblasts and CAFs" in the main methods section for details about how the KPF-derived *Hif2*$^{fl/fl}$ CAF lines were harvested and established. Recombination was induced *ex vivo* via infection with Adeno-Cre-eGFP (VVC-U of Iowa-1174) or control Adeno-eGFP (VVC-U of Iowa-4) at MOI 100. Viral vectors were provided by the University of Iowa Viral Vector Core. (http://www.medicine.uiowa.edu/vectorcore). For single subclone expansion, 500 cells were seeded in 10 cm^2 plates and colonies were allowed to form. Single colonies were picked and expanded, and PCR genotyping was used to validate *Hif2α* recombination in pure subclones[1].

Cell Line Immunofluorescence

For quantitative nuclear HIF1 analysis, HIF2 WT and HIF2 KO CAFs were seeded in cell imaging 8 chamber cover glass slides (Cellvis, C8-1.5H-N) and allowed to attach for 24 h. Cells were subsequently treated with DMSO or FG4592 (50 μM) for 48 hrs. After 48 h, cells were fixed with a 4% solution of PFA in cytoskeleton stabilizing buffer (PEM, 80 mM PIPES pH 6.8, 5 mM EGTA, 2 mM $MgCl_2$) for 15 min at room temperature[3, 4], permeabilized with 0.3% Triton X-100 for 10 min, blocked with 10% goat serum (Millipore Sigma, S26-100ML) for 1h and incubated with primary anti-HIF1α (1:500, Abcam ab179483, RRID:AB_2732807) in dilution/wash buffer (PBS, 1% BSA, 0.1% Tween-20) for 1h at room temperature. Cells were then washed with washed buffer 3 times, incubated with secondary (1:1000, Goat anti-Rabbit 640R, Biotium 20176-1) for 1h at room temperature, rinsed with wash buffer twice, counter stained with

membrane (2 μg/ml, WGA-640R, Biotium 29026-1) and nuclear (1:2000, Hoechst 33342, ThermoFisher, H3570) stain and rinsed with PBS twice before imaging. Cells were imaged with a Ziess LSM 880 confocal microscope using a 63x oil objective. For quantitative nuclear HIF1α analysis, confocal images were opened in NIH's ImageJ software (ImageJ, RRID:SCR_003070; Fiji, RRID:SCR_002285), and a custom macro was used to quantify relative fluorescent intensity of HIF1α in nuclei. Briefly, Hoechst signal was used to define a binary nuclear mask that was applied to HIF1α images. Average fluorescent intensity of the mask images was subsequently recorded.

Quantitative Real-Time Polymerase Chain Reaction

Frozen tumors from KPF CAF-HIF2 WT and KO mice were homogenized and RNA was purified using an RNeasy mini kit (QIAGEN, 74106) and reverse transcription was performed with the QuantiTect reverse transcription kit (QIAGEN, 205313). Quantitative real-time polymerase chain reaction (qRT-PCR) was carried out using a QuantiFast SYBR Green PCR kit (QIAGEN, 204056) on a StepOnePlus real-time PCR system (Applied Biosystems). qRT-PCR analysis was also performed on RAW 264.7 murine macrophages and CAFs treated with the indicated conditions; reverse transcription was performed with the iScript cDNA synthesis kit (Bio-Rad, 170-8891) and qRT-PCR was carried out using iTaq Universal SYBR Green Supermix (Bio-Rad, 172-5124). *Hprt* and *Vcp* were used as reference genes for CAFs; *Ddx54* and *Hsp90b1* were used as reference genes for macrophages. Primers are listed in Supplementary Table 1.

Epithelial HIF1 and HIF2 KO

We isolated epithelial PDAC cells from KPF-HIF1$^{fl/fl}$ or KPF-HIF2$^{fl/fl}$ mice and induced recombination *ex vivo* via infection with Adeno-Cre or control Adeno-GFP. Recombined KPF cells were resuspended in PBS and Matrigel in a 1:1 ratio and orthotopically implanted into the pancreata of immunocompromised mice.

Hematopoietic Toxicity Study

For the hematopoietic toxicity study, 1 x 10^5 KPC cells were resuspended in PBS and Matrigel in a 1:1 ratio and injected orthotopically into the tail of the pancreas of syngeneic 12-week-old C57BL/6 male mice. After 2 weeks of recovery, we began treatment with PT2399 5 days per week, twice daily for 7 weeks, at 50 mg/kg via oral gavage. Terminal blood collection via cardiac puncture was performed at the study endpoint and complete blood count analysis was done at the MD Anderson Department of Veterinary Medicine & Surgery Pathology Core.

Supplementary Figures and Tables:

Supplementary Table 1: PCR and qRT-PCR Primer List	
Gene Target	**Primer Sequence or Catalog #**
Arg1 F	ACAAGACAGGGCTCCTTTCAG
Arg1 R	CTTGGGAGGAGAAGGCGTTT
C3ar1 F	TGCTCAGCAACTCGTCCAAT
C3ar1 F	ATGGAGGCAATGTCTTGGGG
Cd74 F	CTCCTTGGGCCTGTGAAGAA
Cd74 R	GTTACCGTTCTCGTCGCACT
Ddx54 F	ACGCGCACAACCATCTT
Ddx54 R	AGCTTTCCGGTCCCTCT
Hif1a	Bio-Rad, Cat#10025636 (qMmuCID0005501)
Hif2a F	CAGGCAGTATGCCTGGCTAATTCCAGTT
Hif2a R-flox	CTTCTTCCATCATCTGGGATCTGGGACT
Hif2a R-KO	GCTAACACTGTACTGTCTGAAAGAGTAGC
Hsp90b1 F	AAAGGACTTGCGACTCGCC
Hsp90b1 R	ATCAGCTCTGACGAACCCGA
Itgam F	GGCAGCCAGATTGGCTCTTA
Itgam R	GCTTCACACTGCCACCGT
Mmp9 F	CAGCCGACTTTTGTGGTCTTC
Mmp9 R	GTACAAGTATGCCTCTGCCA
Tgfb-1 F	ACCGCAACAACGCCATCTAT
Tgfb-1 R	TGCCGTACAACTCCAGTGAC
Vcp F	TCGGCTATGGAGGTAGAAGA
Vcp R	ATCGCTGACAGAACGTCG
Vegfa F	TTCGTCCAACTTCTGGGCTC
Vegfa R	CTGGGACCACTTGGCATGG

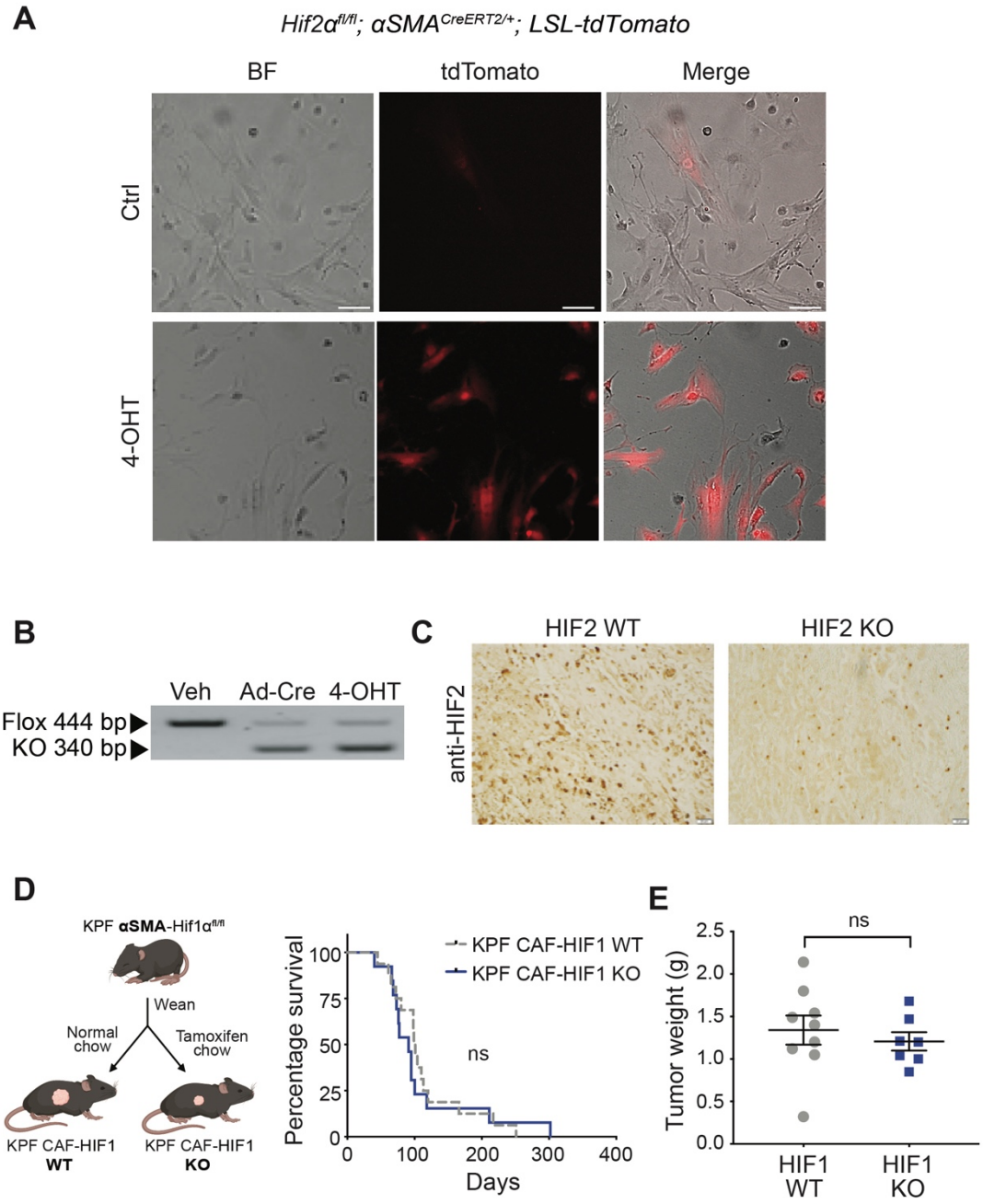

Supplementary Figure 1. Stromal HIF2 but not HIF1 is critical for PDAC progression, Related to Figure 1. *(A and B)* Fibroblasts isolated from the pancreata of *Hif2α$^{fl/fl}$; αSMA$^{CreERT2/+}$; LSL-tdTomato* mice were treated with vehicle DMSO (veh), adenovirus-Cre (Ad-Cre) as a positive control, or 4-hydroxytamoxifen (4-OHT) *ex vivo*. *(A)* Fluorescent microscopy confirmed activation of the Cre-ERT2 fusion protein in activated αSMA+ fibroblasts. Scale bars, 100 μm; BF, bright-field images. *(B)* PCR genotyping confirmed deletion of HIF2. *(C)* Representative IHC images of KPF CAF-HIF2 WT and KO tumors stained for HIF2 (n = 5/group). Scale bars, 20 μm. *(D)* Experimental design to

generate KPF CAF-HIF1 wildtype (WT) control and KPF early CAF-HIF1 KO mice; Kaplan-Meier curves showing percentage survival for KPF CAF-HIF1 WT (n = 16) and KO mice (n = 13). ns (not significant), by log-rank test. *(E)* Corresponding tumor weights for KPF CAF-HIF1 WT (n = 9) and KO mice (n = 7). Mean ± SEM; ns, by Student's *t* test.

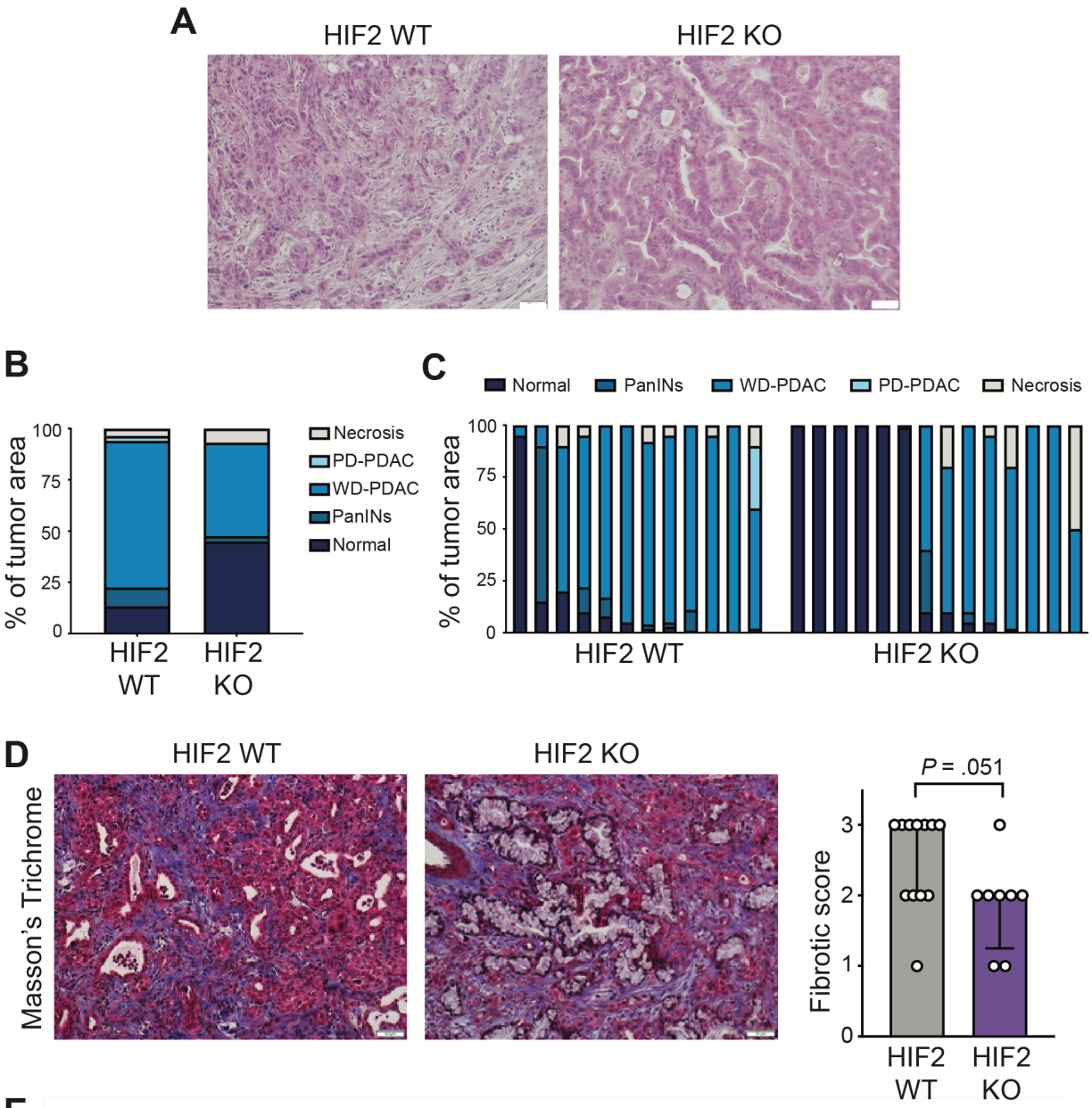

E

Proportion of KPF CAF-HIF2 WT and KO mice with metastasis

Group	Mice presenting with metastasis	Total mice necropsied	Metastasis rate	Statistical Analysis
HIF2 WT	9	20	0.45	*P* = .514
HIF2 KO	6	19	0.32	

Supplementary Figure 2. Histopathological analyses of PDAC tumors with CAF-specific HIF2 ablation, Related to Figure 1. *(A)* Representative images of H&E-stained KPF CAF-HIF2 WT (n = 12) and KO (n = 14) tumors. Scale bars, 50 μm. *(B and C)* Quantification of the differentiation state of the tumors in *(A)*. The fractions of

each pancreas that were necrotic tissue, poorly differentiated PDAC (PD-PDAC), well-differentiated PDAC (WD-PDAC), pancreatic intraepithelial neoplasia (PanIN), or normal tissue were scored in a blinded manner, and values are shown averaged per group *(B)* or shown per individual mouse *(C). (D) Left:* Representative images of Masson's trichrome staining in KPF CAF-HIF2 WT (n = 12) and KO (n = 8) tumors; scale bars, 50 μm. *Right:* Fibrotic score; median ± interquartile range; *P*, by Mann–Whitney *U* test. *(E)* Proportion of KPF CAF-HIF2 WT and KO mice presenting distant metastasis; *P*, by Fisher's exact test.

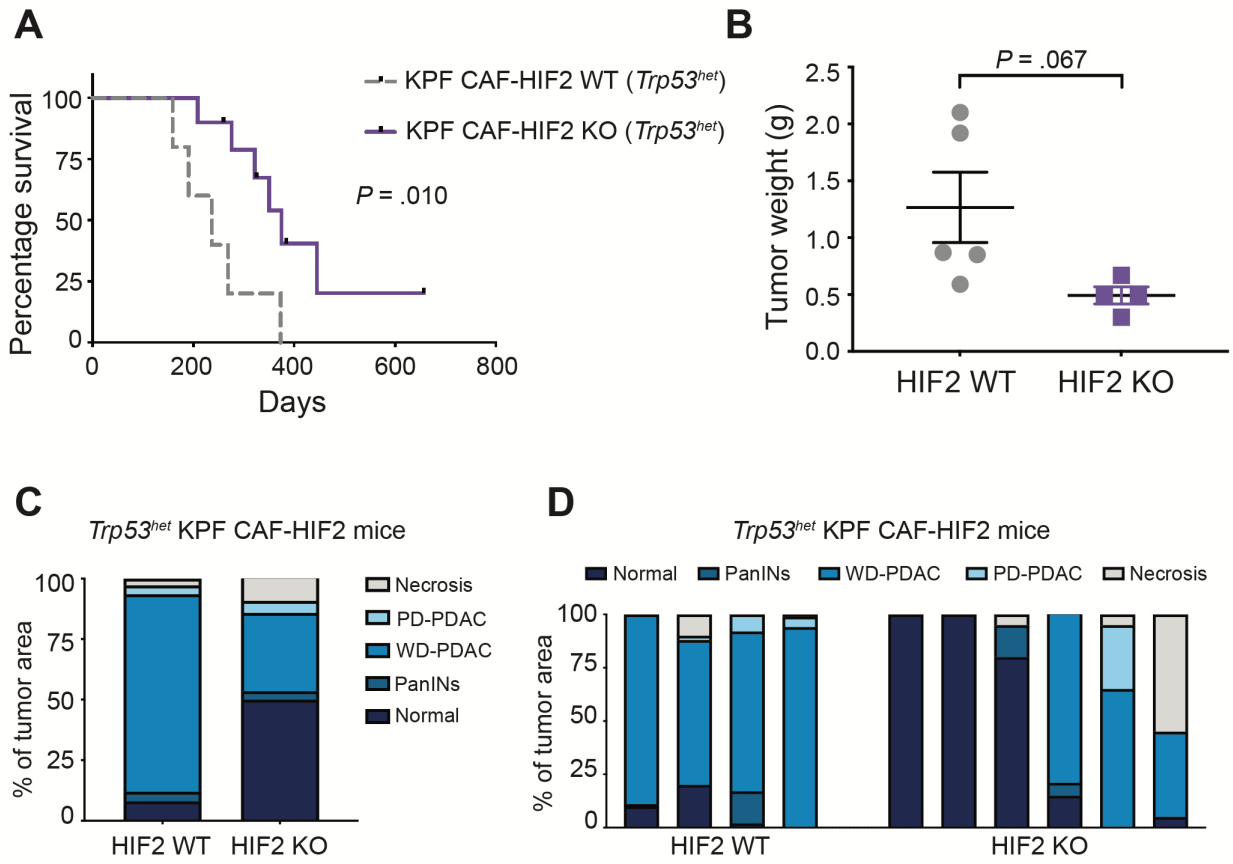

E

Proportion of Trp53 het KPF CAF-HIF2 WT and KO mice with metastasis

Group	Mice presenting with metastasis	Total mice necropsied	Metastasis rate	Statistical analysis
HIF2 WT	2	5	0.40	*P* = .152
HIF2 KO	0	7	0.00	

Supplementary Figure 3. Histopathological analyses of *Trp53* heterozygous PDAC tumors with CAF-specific HIF2 ablation, Related to Figure 1. *(A)* Kaplan-Meier curves showing percentage survival for *Trp53* heterozygous (*Trp53*^{het}) KPF CAF-HIF2 WT (n = 5) and KO mice (n = 10). *P*, by log-rank test. *(B)* Corresponding tumor weights for KPF CAF-HIF2 WT (n = 5) and KO mice (n = 4). Mean ± SEM; *P*, by Student's *t* test. *(C and D)* Quantification of the differentiation state of the tumors in *(A and B)*. The fractions of each pancreas that were necrotic tissue, poorly differentiated PDAC (PD-PDAC), well-differentiated PDAC (WD-PDAC), pancreatic intraepithelial neoplasia (PanIN), or normal tissue were scored in a blinded manner, and values are shown averaged per group *(C)* or shown per individual mouse *(D)*; n = 4-6 mice/group. *(E)* Proportion of KPF CAF-HIF2 WT and KO mice presenting distant metastasis; *P*, by Fisher's exact test.

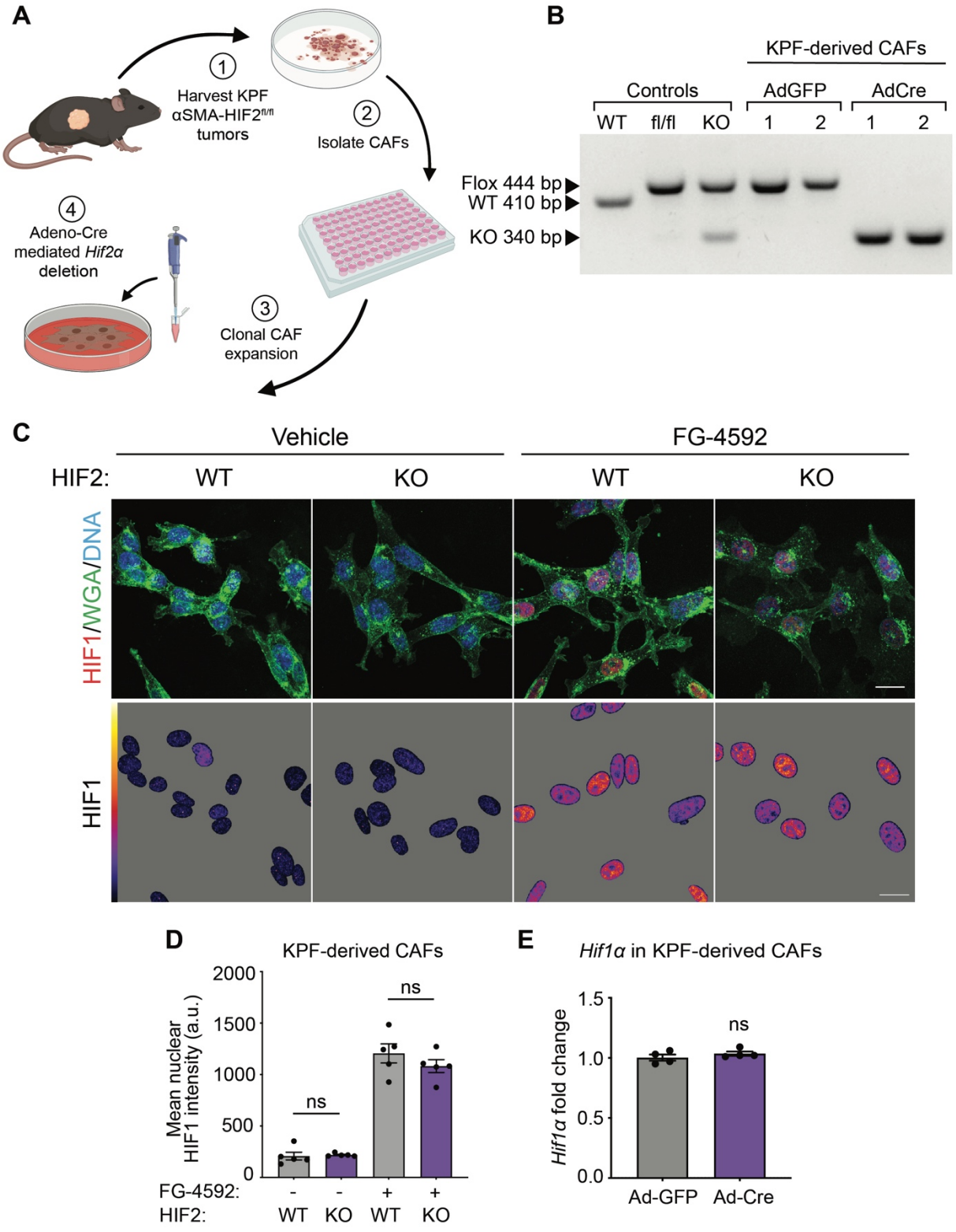

Supplementary Figure 4. HIF2 KO in CAFs does not alter HIF1 expression, Related to Figure 1. *(A) Hif2α*$^{fl/fl}$ CAFs were isolated from KPF tumors using a combination of enzymatic digestion, outgrowth, and clonal isolation. CAFs were validated prior to being

infected with adenovirus-GFP (Ad-GFP) or adenovirus-Cre (Ad-Cre) to generate HIF2 WT and HIF2 KO CAFs, respectively. *(B)* Single HIF2 WT and HIF2 KO CAF subclones were expanded and PCR genotyping was used to confirm deletion of HIF2. *(C)* Representative IF images of HIF2 WT and HIF2 KO CAFs treated with vehicle or FG-4592 showing merged maximum intensity projection *(top)* and masked nuclear HIF1 *(bottom).* Scale bars, 20 μm. *(D)* Quantitative analysis of mean nuclear HIF1 intensity per field of view (FOV; n = 5 FOVs/group). *(E) Hif1α* expression was measured by qRT-PCR. Data is representative of two independent experiments. All error bars represent mean ± SEM; *P*, by Student's *t* test.

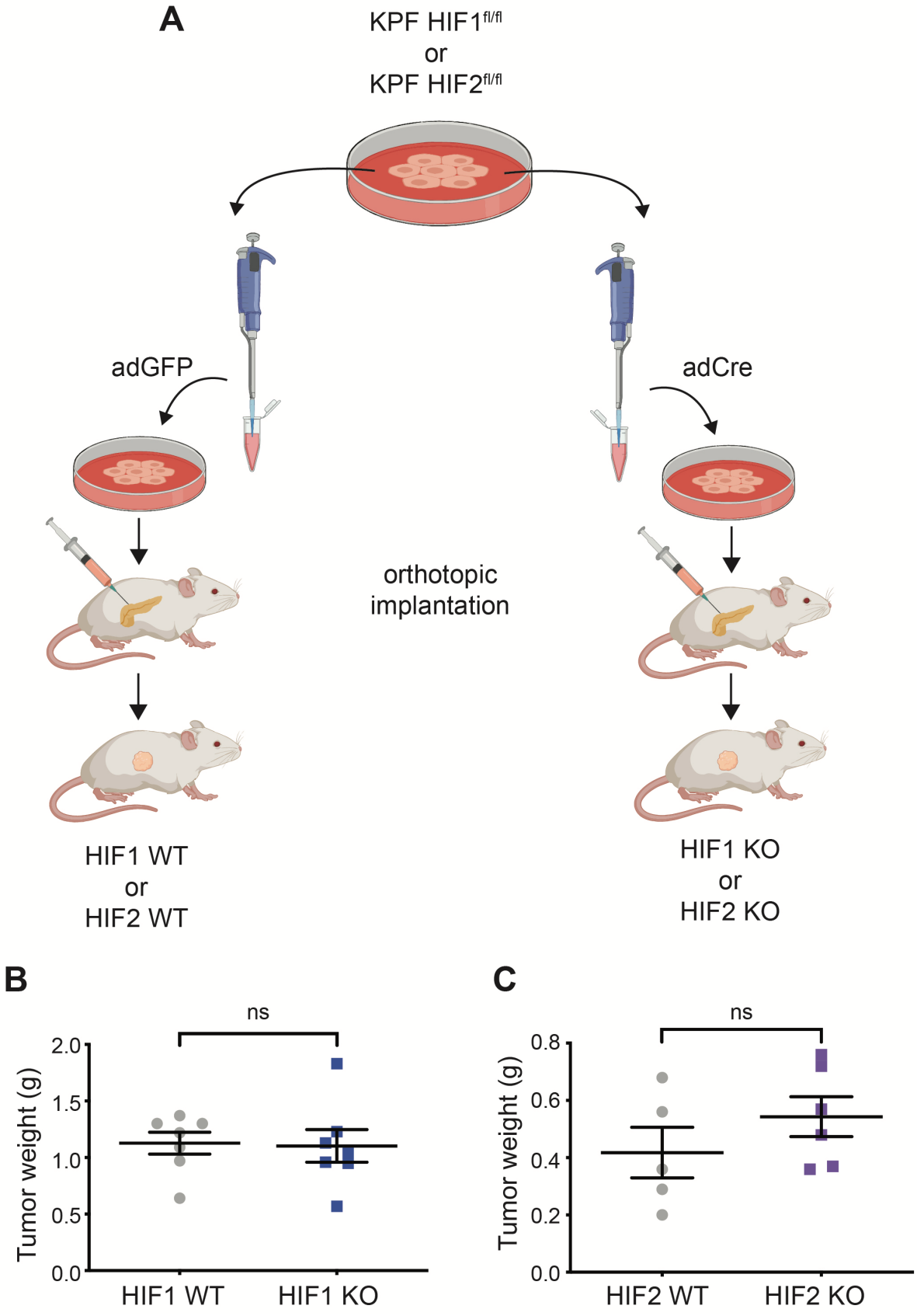
A
KPF HIF1fl/fl
or
KPF HIF2fl/fl
adGFP
adCre
orthotopic
implantation
HIF1 WT
or
HIF2 WT
HIF1 KO
or
HIF2 KO
B
ns
Tumor weight (g)
2.0
1.5
1.0
0.5
0.0
HIF1 WT
HIF1 KO
C
ns
Tumor weight (g)
0.8
0.6
0.4
0.2
0.0
HIF2 WT
HIF2 KO

Supplementary Figure 5. KPF pancreatic cancer cell-specific HIF1 or HIF2 knockout does not affect PDAC progression, Related to Figure 1. *(A)* Cancer cells from KPF *Hif1α*$^{fl/fl}$ or *Hif2α*$^{fl/fl}$ tumors were isolated and infected *ex vivo* with Ad-GFP or Ad-Cre and subsequently injected into the pancreata of immunocompromised mice. *(B and C)* Comparison of the orthotopic tumors showed no significant difference in tumor size between tumors with *(B) Hif1α* or *(C) Hif2α* deletion and the respective WT controls. Mean ± SEM; ns, by Student's *t* test.

A

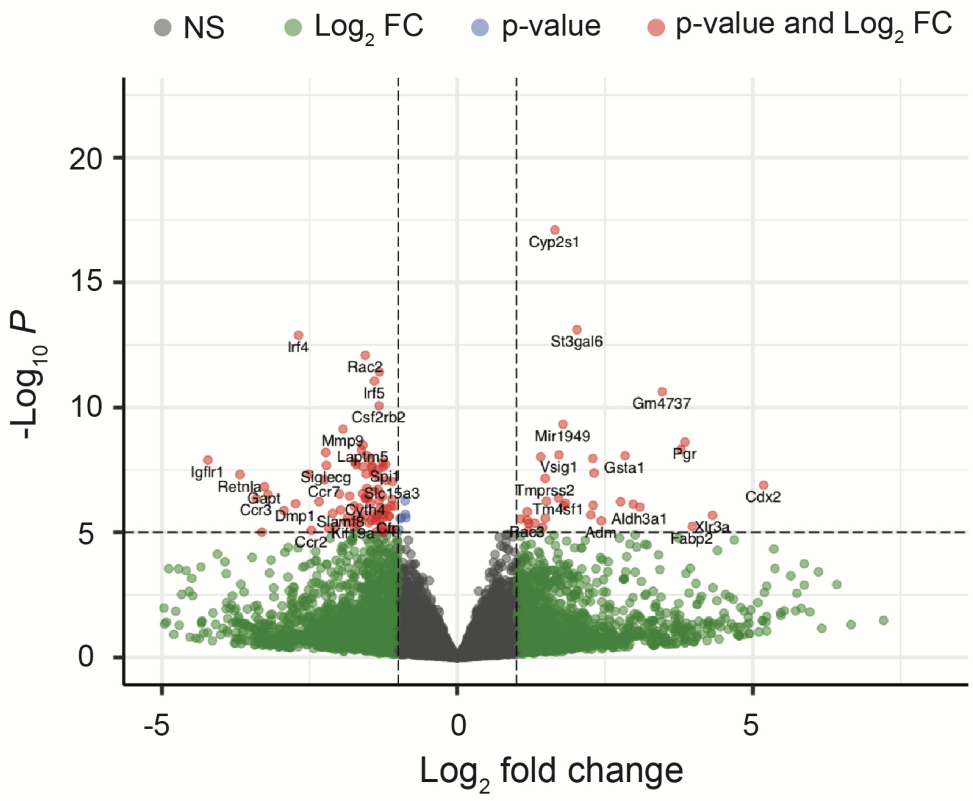

B

Enriched in KPF CAF-HIF2 WT tumors (compared to KPF CAF-HIF2 KO tumors)

Rank	Gene set	MSigDB Collection	NES	Nom p-value	FDR q-value
1	REACTOME_DAP12_SIGNALING	C2	2.15	.000	.014
2	REACTOME_INTEGRIN_SIGNALING	C2	2.06	.000	.023
3	KEGG_FC_GAMMA_R_MEDIATED_PHAGOCYTOSIS	C2	1.98	.000	.020
4	GO_REGULATION_OF_LYMPHOCYTE_MEDIATED_IMMUNITY	C5	1.88	.000	.091
5	GO_MYELOID_CELL_APOPTOTIC_PROCESS	C5	1.85	.000	.088
6	HALLMARK_KRAS_SIGNALING_UP	H	1.83	.000	.040
7	GO_REGULATION_OF_MYELOID_LEUKOCYTE_MEDIATED_IMMUNITY	C5	1.81	.034	.077
8	HALLMARK_INFLAMMATORY_RESPONSE	H	1.80	.000	.043
9	GO_RESPIRATORY_BURST	C5	1.79	.000	.081
10	GO_MACROPHAGE_ACTIVATION	C5	1.78	.000	.084
11	GO_POSITIVE_REGULATION_OF_INTERLEUKIN_12_PRODUCTION	C5	1.76	.000	.084
12	GO_MACROPHAGE_DIFFERENTIATION	C5	1.76	.000	.085
13	GO_POSITIVE_REGULATION_OF_TUMOR_NECROSIS_FACTOR_SUPERFAMILY_CYTOKINE_PRODUCTION	C5	1.75	.000	.085
14	GO_INTERLEUKIN_10_PRODUCTION	C5	1.74	.000	.090
15	GO_DENDRITIC_CELL_MIGRATION	C5	1.71	.000	.098
16	GO_POSITIVE_REGULATION_OF_INTERLEUKIN_6_PRODUCTION	C5	1.69	.032	.104
17	GO_POSITIVE_REGULATION_OF_INTERLEUKIN_4_PRODUCTION	C5	1.65	.000	.127
18	GO_INTERLEUKIN_1_BETA_PRODUCTION	C5	1.62	.000	.145
19	GO_NEGATIVE_REGULATION_OF_CELLULAR_RESPONSE_TO_TRANSFORMING_GROWTH_FACTOR_BETA_STIMULUS	C5	1.61	.000	.085
20	GO_REGULATION_OF_MACROPHAGE_MIGRATION	C5	1.60	.020	.161

Supplementary Figure 6. Stromal HIF2 regulates tumor macrophage recruitment, Related to Figure 2. *(A)* Volcano plot illustrating differential gene expression analysis using bulk RNA-seq data from KPF CAF-HIF2 tumors (n = 4/group). *(B)* Gene sets enriched in KPF CAF-HIF2 WT tumors compared to KO tumors ranked by normalized enrichment score (NES). Gene set enrichment analysis was performed using bulk RNA-seq data from *(A)*. Nom., nominal; FDR, false discovery rate.

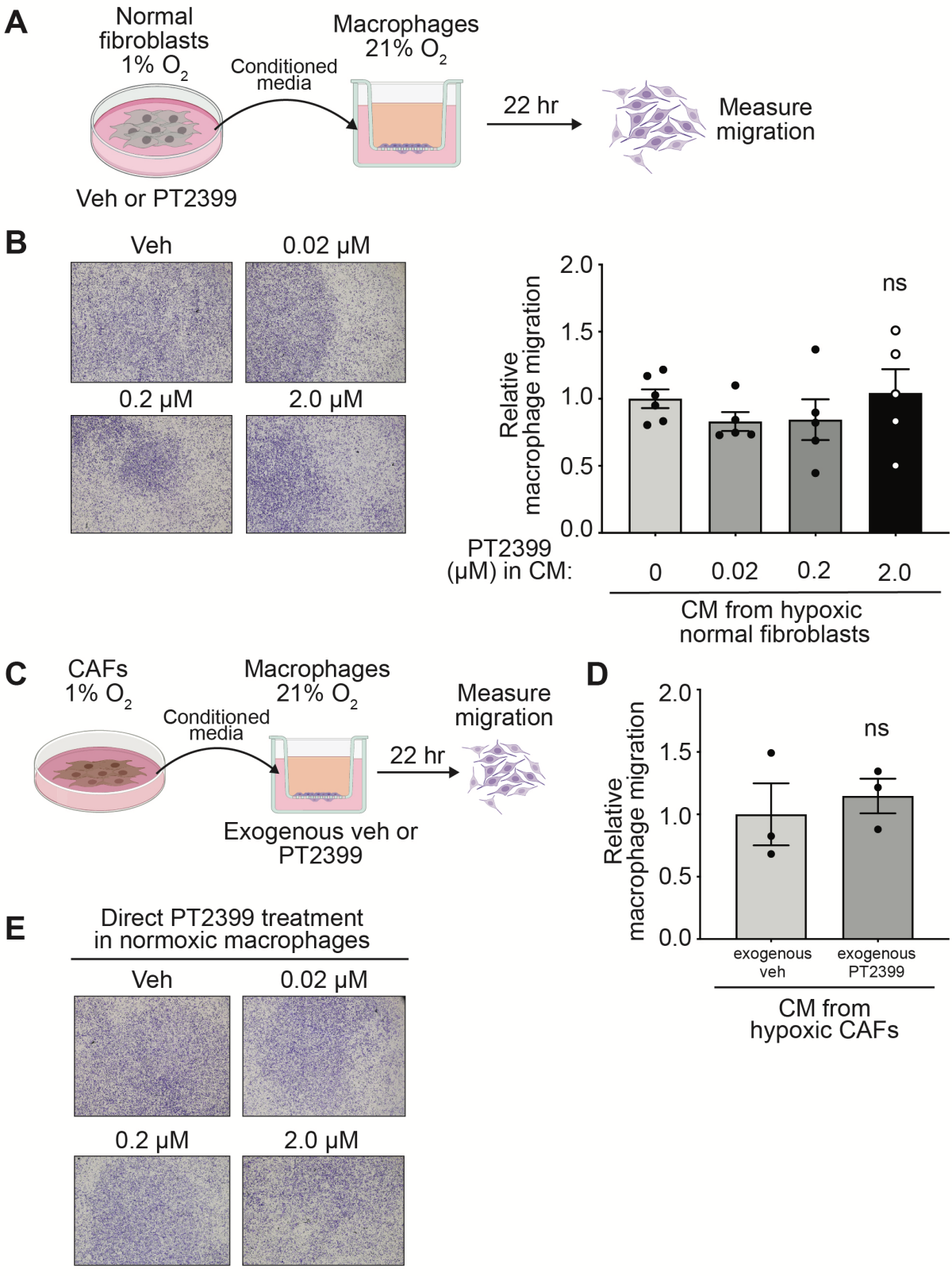

Supplementary Figure 7. Hypoxic CAFs promote macrophage migration in a HIF2-dependent paracrine fashion, Related to Figure 3. *(A)* Conditioned media (CM) was collected from hypoxic normal fibroblasts treated with vehicle (veh) or PT2399. This CM

was subsequently placed in the bottom chamber of a transwell as a chemoattractant for macrophage migration. *(B)* Representative bright-field images (stitched whole well; *left*) and quantification of macrophage migration relative to macrophages treated with CM from hypoxic veh-treated normal fibroblasts (*right*) of the transwell assay depicted in *(A)*; (n = 5/group pooled from 2 independent experiments). *(C)* CM was collected from hypoxic CAFs. Vehicle or PT2399 was then exogenously added to the processed CM, which was subsequently placed in the bottom chamber of a transwell as a chemoattractant for macrophage migration. *(D)* Quantification of macrophage migration relative to macrophages treated with CM from hypoxic CAFs with exogenous veh of the transwell assay depicted in *(C)*. *(E)* Representative bright-field images (stitched whole well) of transwell migration experiment described in Figure 3C-D. 5%FBS/DMEM with veh or PT2399 was used as chemoattractant for macrophage migration. All error bars represent mean ± SEM; *P*, by one-way ANOVA *(B)* or Student's *t* test *(D)*; ns, not significant.

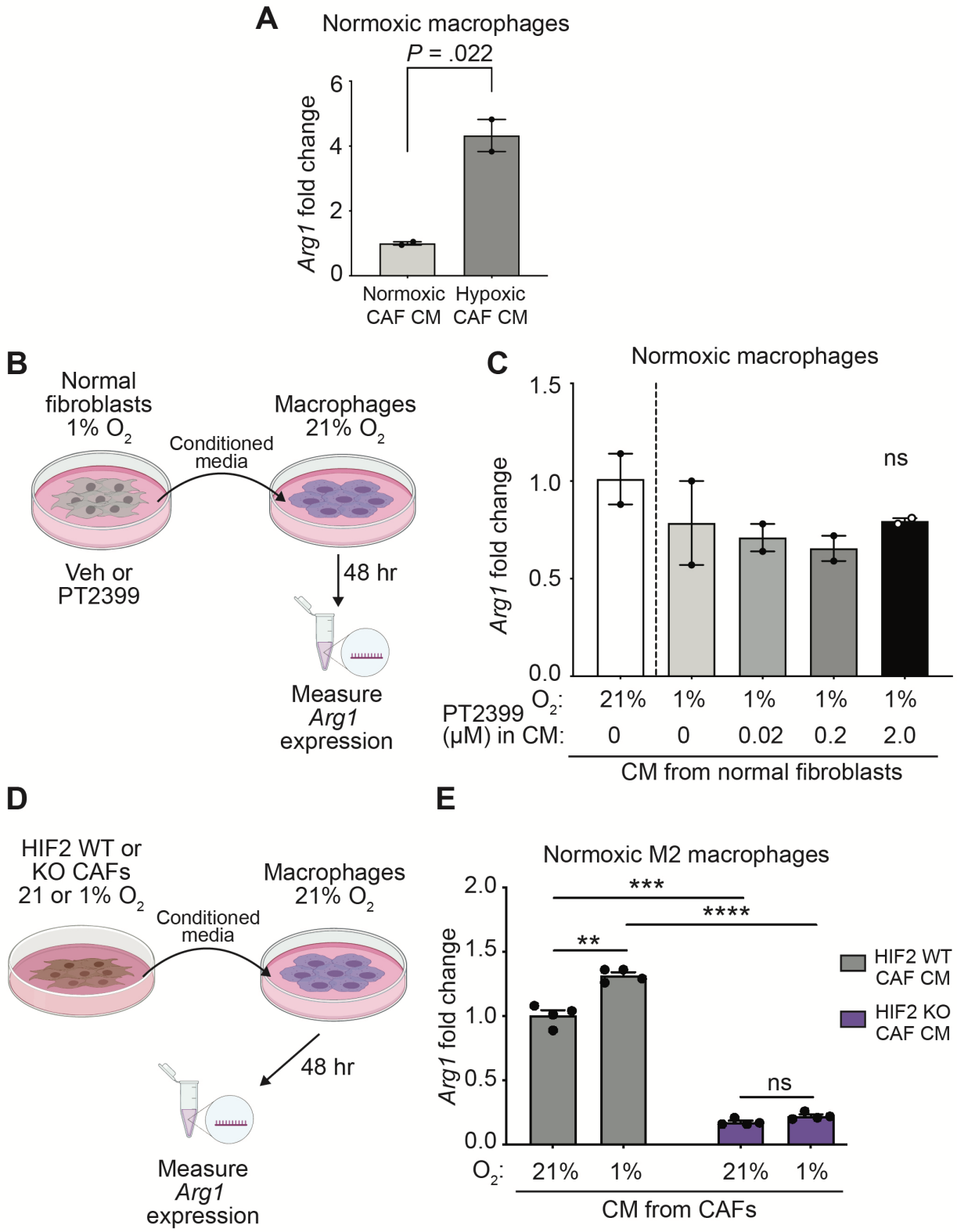

Supplementary Figure 8. Hypoxic CAFs promote macrophage activation and M2 polarization in a HIF2-dependent paracrine fashion, Related to Figure 4. *(A)* Macrophages were incubated under normoxic conditions with CM collected from CAFs

grown in normoxic or hypoxic conditions and *Arg1* expression was measured by qRT-PCR. *Arg1* fold change over macrophages incubated with CM from normoxic CAFs is shown. *(B)* Macrophages were incubated under normoxic conditions with CM collected from hypoxic normal fibroblasts treated with vehicle or PT2399 and *Arg1* expression was measured by qRT-PCR. (*C*) *Arg1* fold change over macrophages incubated with CM from vehicle-treated normoxic normal fibroblasts is shown. (*D*) Macrophages were incubated under normoxic conditions with CM collected from normoxic or hypoxic HIF2 WT and HIF2 KO CAFs and *Arg1* expression was measured by qRT-PCR. (*E*) *Arg1* fold change over macrophages incubated with CM from normoxic HIF2WT CAFs is shown. All error bars represent mean ± SEM; *P*, by Student's *t* test; $^{**}P \leq .01$, $^{***}P \leq .001$, $^{****}P \leq .0001$; ns, not significant.

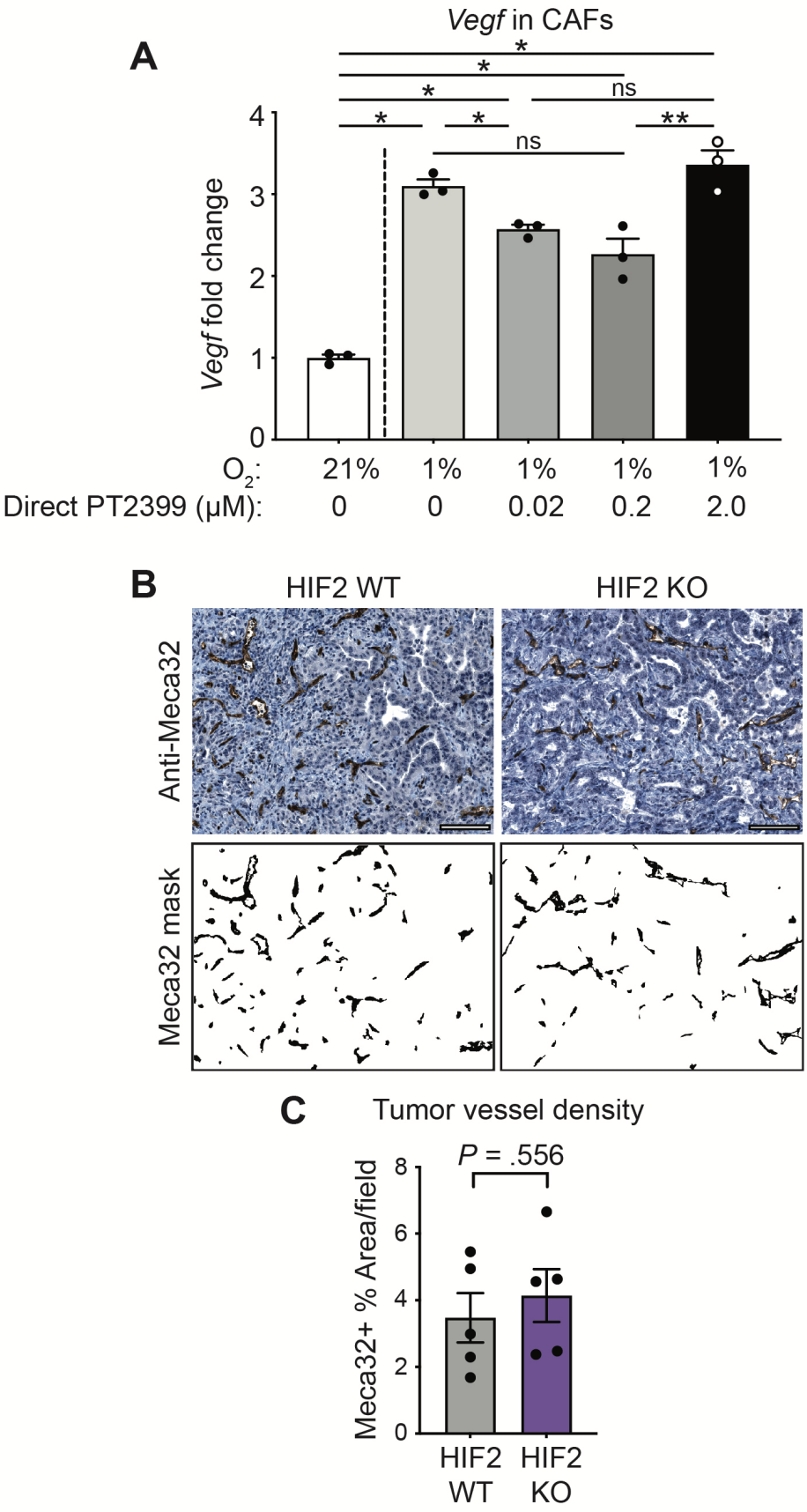
A
Vegf in CAFs
Vegf fold change
0
1
2
3
4
*
*
*
*
*
ns
ns
**
O2:
21%
1%
1%
1%
1%
Direct PT2399 (μM):
0
0
0.02
0.2
2.0
B
HIF2 WT
HIF2 KO
Anti-Meca32
Meca32 mask
C
Tumor vessel density
P = .556
Meca32+ % Area/field
0
2
4
6
8
HIF2 WT
HIF2 KO

Supplementary Figure 9. Assessment of CAF-HIF2 signal abrogation on *Vegf* levels and tumor vessel density, Related to Figure 4. *(A)* CAFs were grown in normoxic or hypoxic conditions and treated with PT2399 at the indicated doses, then *Vegfa* expression was measured by qRT-PCR. *(B)* Representative IHC (*top*) and masked images (*bottom*) of KPF CAF-HIF2 tumors stained for Meca32 (n = 5/group); scale bars, 100 μm. (*C*) Quantification of Meca32+ percent area per field. Each data point represents one mouse, with two random fields of view analyzed and averaged per mouse. All error bars represent mean ± SEM; *P*, by Student's *t* test *(C*) or one-way ANOVA *(A);* $*P \leq .05$, $**P \leq .01$.

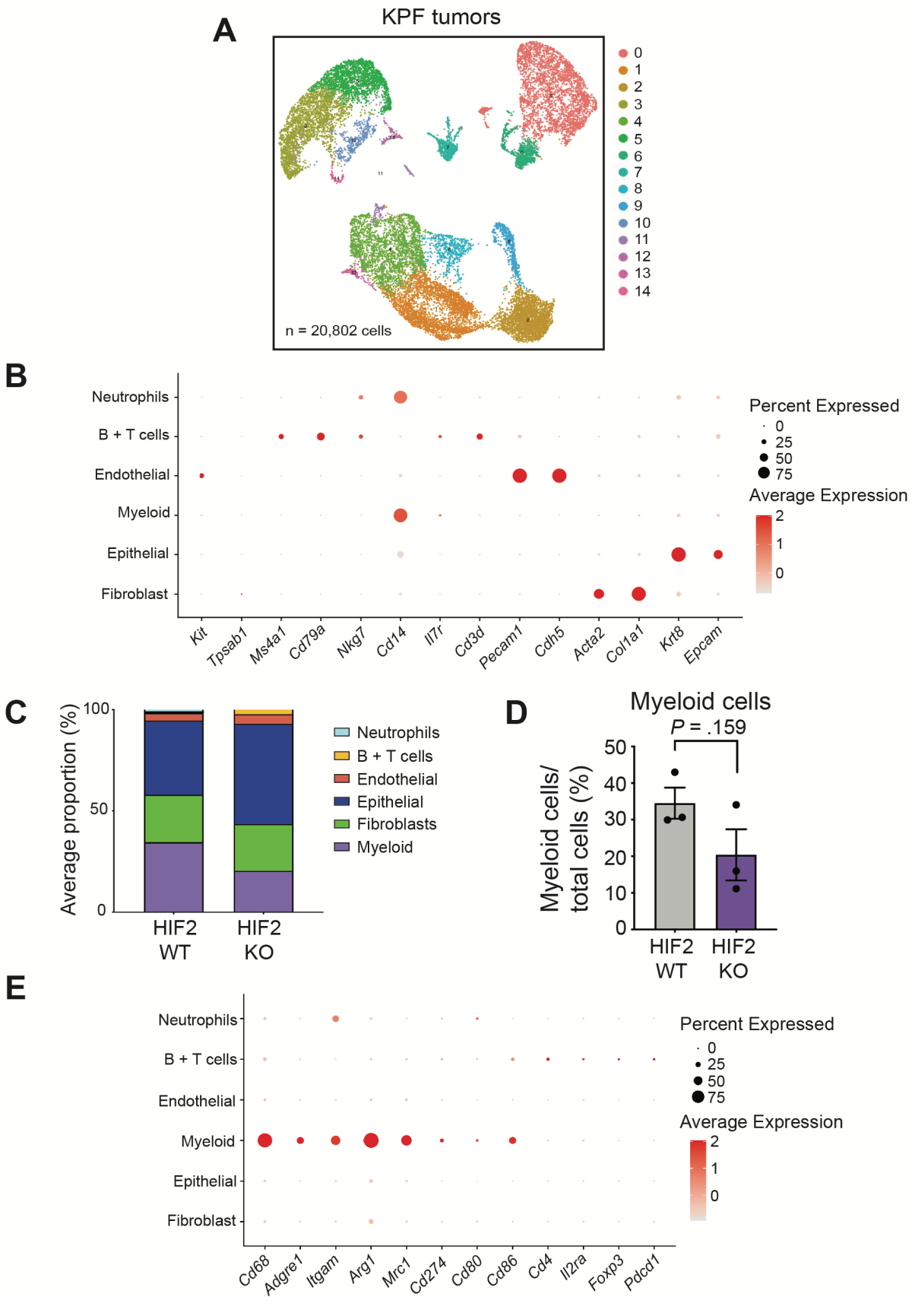
A
KPF tumors
n = 20,802 cells
0
1
2
3
4
5
6
7
8
9
10
11
12
13
14
B
Neutrophils
B + T cells
Endothelial
Myeloid
Epithelial
Fibroblast
Kit
Tpsab1
Ms4a1
Cd79a
Nkg7
Cd14
Il7r
Cd3d
Pecam1
Cdh5
Acta2
Col1a1
Krt8
Epcam
Percent Expressed
0
25
50
75
Average Expression
2
1
0
C
Average proportion (%)
100
50
0
HIF2 WT
HIF2 KO
Neutrophils
B + T cells
Endothelial
Epithelial
Fibroblasts
Myeloid
D
Myeloid cells
P = .159
Myeloid cells/ total cells (%)
50
40
30
20
10
0
HIF2 WT
HIF2 KO
E
Neutrophils
B + T cells
Endothelial
Myeloid
Epithelial
Fibroblast
Cd68
Adgre1
Itgam
Arg1
Mrc1
Cd274
Cd80
Cd86
Cd4
Il2ra
Foxp3
Pdcd1
Percent Expressed
0
25
50
75
Average Expression
2
1
0

Supplementary Figure 10. Stromal HIF2 ablation reduces the PDAC immunosuppressive landscape, Related to Figure 5. *(A)* UMAP of scRNA-seq analysis of 20,802 cells sorted from 6 mice (3/group). Graph-based clustering identified 15 clusters, indicated by color. *(B)* Bubble plots showing the relative average expression of selected cell-type-specific markers across all major cell populations identified in the scRNA-seq analysis. The size of the dots indicates the percentage of the cell population that expressed the marker, and the intensity of color indicates the average expression level. *(C)* Proportions of cell types in CAF-HIF2 WT and KO tumors, quantified as an average per group. *(D)* Average percentage of myeloid cells over total cells sequenced per tumor. Error bars represent mean ± SEM. *(E)* Bubble plots showing the relative average expression of macrophage and Treg markers across all major cell populations identified in the scRNA-seq analysis. The size of the dots indicates the percentage of the cell population that expressed the marker, and the intensity of color indicates the average expression level.

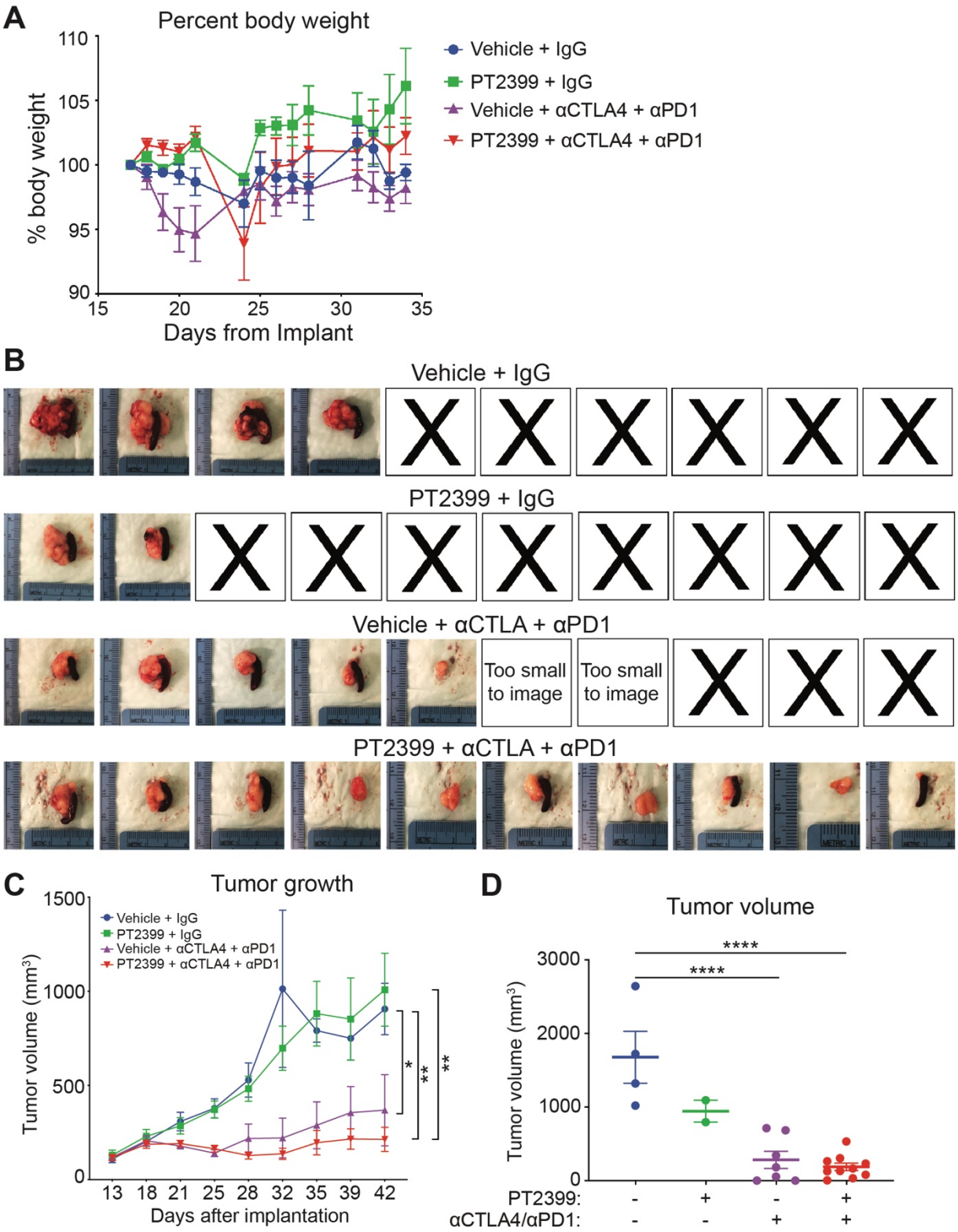

Supplementary Figure 11. Gross and tumor burden analyses of immunotherapy experiment in orthotopic KPC model, Related to Figure 6. *(A)* Percentage body weight of syngeneic orthotopic KPC mice treated with PT2399 + αCTLA4/αPD1 (n =

10/group). *(B)* Images of gross tumors with spleen attached. Mice that were found dead are marked with an X. *(C)* Corresponding tumor growth curve. Tumors were measured by ultrasound. *P*, by Mann–Whitney *U* test. *(D)* Tumor volumes measured by caliper at the time of sacrifice. Mean ± SEM; *P*, by one-way ANOVA; **P* ≤ .05, ***P* ≤ .01, ****P* ≤ .001, ****P ≤ .0001

Proportion of orthotopic KPC model mice with metastasis

Group	Mice presenting with metastasis	Total mice necropsied	Metastasis rate	Statistical Analysis
Veh + IgG	2	4	0.50	-
PT2399 + IgG	5	7	0.71	*P* = .576
Veh + DCB	1	7	0.14	*P* = .491
PT2399 + DCB	1	10	0.10	*P* = .176

Supplementary Figure 12. Proportion of orthotopic KPC model mice with metastasis, Related to Figure 6. *P*, by Fisher's exact test.

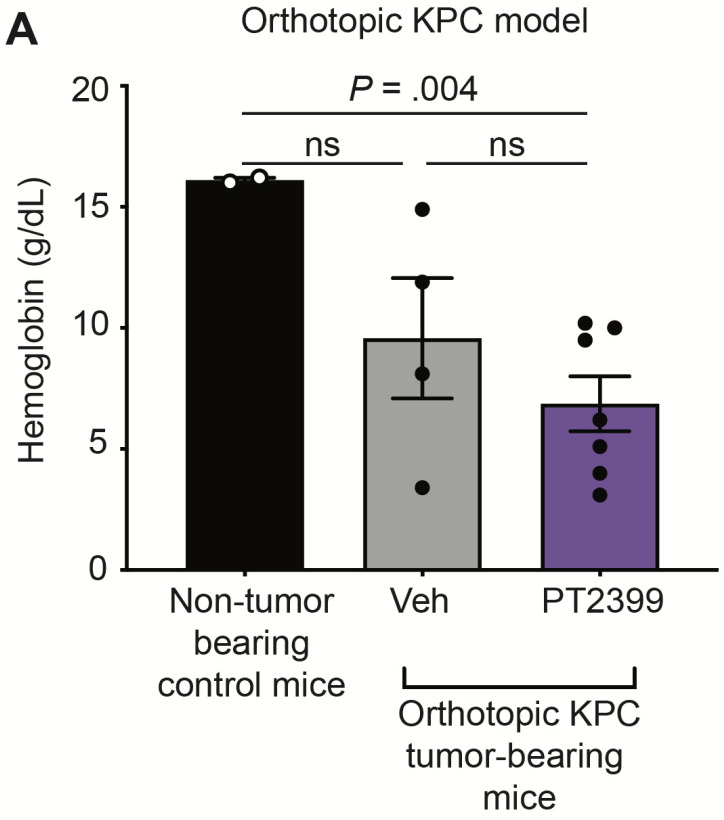
A
Orthotopic KPC model
P = .004
ns
ns
Hemoglobin (g/dL)
20
15
10
5
0
Non-tumor bearing control mice
Veh
PT2399
Orthotopic KPC tumor-bearing mice

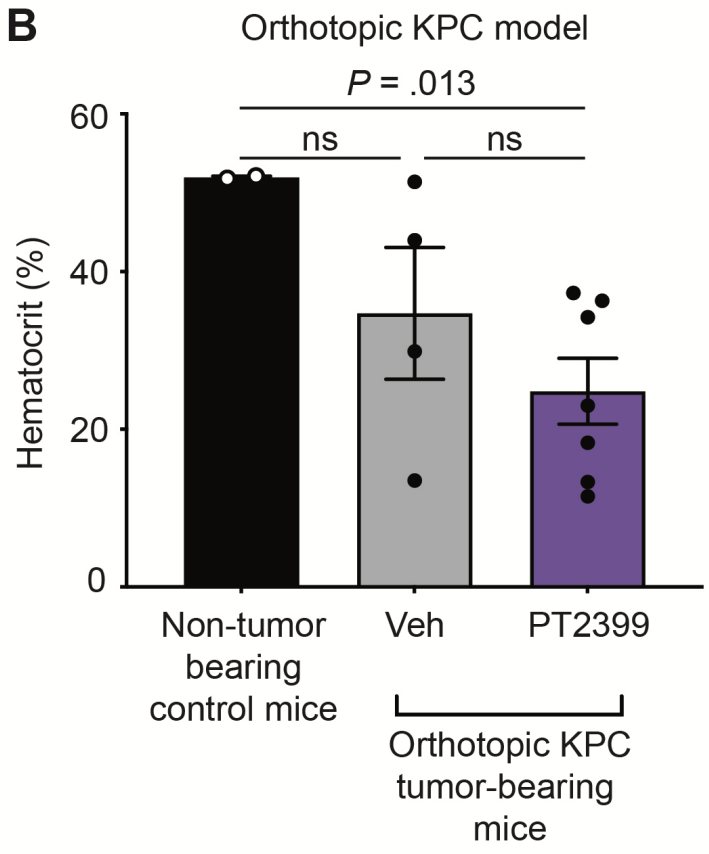
B
Orthotopic KPC model
P = .013
ns
ns
Hematocrit (%)
60
40
20
0
Non-tumor bearing control mice
Veh
PT2399
Orthotopic KPC tumor-bearing mice

Supplementary Figure 13. On-target bone marrow toxicity of pharmacological HIF2 inhibition with PT2399 in tumor bearing mice, Related to Figure 6. A syngeneic orthotopic KPC mouse model was used to assess bone marrow toxicity related to systemic HIF2 inhibition. Mice were treated with treated with veh or PT2399 and non-tumor bearing C57BL/6 mice were used as a control. *(A)* Hemoglobin and hematocrit levels *(B)* are shown (n = 2-7 mice/group). All error bars represent mean ± SEM; *P,* by Student's *t* test; ns, not significant.

Supplementary References:

1. Gruber M, Hu C-J, Johnson RS, et al. Acute postnatal ablation of Hif-2α results in anemia. Proceedings of the National Academy of Sciences 2007;104:2301.
2. Fujimoto TN, Colbert LE, Huang Y, et al. Selective EGLN Inhibition Enables Ablative Radiotherapy and Improves Survival in Unresectable Pancreatic Cancer. Cancer Res 2019;79:2327-2338.
3. Pereira PM, Albrecht D, Culley S, et al. Fix Your Membrane Receptor Imaging: Actin Cytoskeleton and CD4 Membrane Organization Disruption by Chemical Fixation. Frontiers in Immunology 2019;10:675.
4. Leyton-Puig D, Kedziora KM, Isogai T, et al. PFA fixation enables artifact-free super-resolution imaging of the actin cytoskeleton and associated proteins. Biology Open 2016;5:1001-1009.